Precise Orbit Determination for Mars Global Surveyor During Hiatus and SPO

F. G. Lemoine[*],
D.D. Rowlands, G. A. Neumann[†], D. E. Smith
Laboratory for Terrestrial Physics
NASA Goddard Space Flight Center
Greenbelt, Maryland

D. E. Pavlis, D. S. Chinn, S. B. Luthcke
Raytheon ITSS, Greenbelt, Maryland

Abstract

The Mars Global Surveyor (MGS) spacecraft arrived at Mars on September 12, 1997. The Mars Orbiting Laser Altimeter (MOLA) collected data during the Hiatus Phase from October 13 to November 7, 1997, and during the Science Phasing Orbit(SPO) in March to April 1998, and June to July 1998. The Doppler tracking data acquired from the Deep Space Network (DSN) were used to compute orbits for the MOLA Science Team. After development of tuned gravity models to 70x70 in spherical harmonics with the MGS tracking data, the RMS radial orbit difference of overlapping MGS arcs during SPO had an overlap consistency of 30 to 35 m, compared to 160 to 200 m with the *a priori* GMM-1 solution. We also demonstrate that the use of altimeter crossovers derived from MOLA altimetry improved the MGS orbits in SPO-1 (March 27 - May 1, 1998) by 15 percent (2.8 m) in the radial component, and 60 percent (600 m) in total position.

INTRODUCTION

The Mars Global Surveyor spacecraft arrived at Mars on September 12, 1997. The initial plans called for three to four months of aerobraking to circularize the orbit by January 1998. Concerns with the -Y panel solar array led to the suspension of aerobraking in October 1997, and an alternate plan to reach the mapping orbit by February of 1999[1]. Aerobraking resumed from November 1997 to March 1998, at a reduced rate[2]. After the end of the first phase of aerobraking, the spacecraft was located in an orbit with a period of 11 hours and 38 minutes, and a mean periapse altitude of 171 km from March 27, 1998 to September 23, 1998. Interim science observations were collected by the MGS instruments in the Science Phasing Orbit-1 (SPO-1; from March 27 to May 1, 1998) and Science Phasing Orbit-2 (SPO-2; May 28 to Sept. 23, 1998), as well as in Hiatus Phase (October - November 1997).

A primary goal for the Mars Orbiter Laser Altimeter (MOLA) is to derive a global, geodetically referenced, 0.2° x 0.2° topographic grid of Mars with a vertical accuracy of better than 30 meters[3].

*Code 926, Laboratory for Terrestrial Physics, NASA Goddard Space Flight Center, Greenbelt, MD 20771; E-mail: flemoine@olympus.gsfc.nasa.gov

†Also at Department of Earth, Atmospheric, and Planetary Sciences, Massachussetts Institute of Technology, Cambridge, MA 02139-4307.

Table 1: MGS Orbit Characteristics during MOLA Data Acquisition

Mission Phase	Dates	Orbital Period (hr)	Periapsis Ht. (km)	Periapsis Latitude (deg)
Insertion	September 12-16, 1997	44.993	263	31° N
Hiatus	Oct. 13 - Nov. 7, 1997	35.43	170	35° N
SPO-1	March 27 - May 1, 1998	11.64	171	61° - 71° N
SPO-2	May 28 - July 30, 1998	11.64	171	82° - 86.3° N 86.3° - 76° N

Topographic mapping of the entire planet will occur after the MGS orbit is circularized at the end of aerobraking. Nevertheless, MOLA collected data during the Hiatus, SPO-1, and the first two months of SPO-2. A single pass of MOLA data was also obtained after Mars Orbit Insertion (MOI), on September 15, 1997. The orbit characteristics for the insertion, Hiatus, and SPO orbits are summarized in Table 1. All these orbits are highly eccentric, so that MOLA data were obtained only for 20 to 30 minutes during each periapsis pass.

The instrument acquired data whenever the spacecraft was below about 785 km, at a rate of 10 Hz. Under the best of conditions, the MOLA data have a precision of 37.5 cm, when the surface slope is less than 2.0° and when the instrument is pointing at nadir[3,4]. Off-nadir data were collected during spacecraft roll-outs, and specially targeted off nadir passes including the campaign to map the northern Mars polar cap during SPO-2. The argument of periapsis of the MGS orbit precessed from 146° in October 1997 to 76° on July 30, 1998, so that periapsis was located exclusively in the Northern Hemisphere when MOLA measurements were made. A total of 2.6 million MOLA ranges were obtained over 208 passes in Insertion, Hiatus, and SPO.

In order to properly analyze the MOLA data, the spacecraft orbit must be known to an accuracy comparable to the performance of the altimeter. Careful attention must be made in the reduction of the DSN tracking data to both the measurement and spacecraft force modeling. The principal concerns in the force modelling include the Mars gravity field perturbations, atmospheric drag, solar radiation pressure, and the periodic angular momentum desaturations. Detailed modeling of the nonconservative forces requires that the spacecraft attitude and shape be properly modelled. The main concerns of the measurement model include proper modelling of the ramped two-way DSN Doppler data, and the one-way Doppler data obtained from the MGS Ultrastable Oscillator (USO)[5]. The offsets of the antenna from the spacecraft center of mass must be included, especially for the one-way data. Each of these issues is explored in this paper, after a brief review of the available data.

MGS TRACKING DATA AND STATION COMPLEMENT

During Hiatus, aerobraking, and SPO-1 and SPO-2, the MGS spacecraft was tracked by the antennae of the Deep Space Network (DSN) using two-way and three-way ramped Doppler and two-way ramped range data. All data were obtained at X band. The ramped Doppler observable is described by Moyer[6,7], and has been used on previous interplanetary space missions, such as Magellan and Voyager. MGS used unramped Doppler during cruise to Mars, but switched to ramped Doppler at the start of aerobraking in September 1997 for operational reasons[8].

Since the High Gain Antenna (HGA) is fixed to the spacecraft prior to the deployment of the antenna arm during mapping, no direct tracking data can be obtained from the HGA while the instrument panel is pointed toward nadir during passage through periapsis, unless fortuitously the HGA is pointed within 3-4° of Earth. During SPO-1, the HGA was aimed from 20° to 50° off of Earth point during the periapse pass, and in early SPO-2 the geometry was even more unfavorable[8]. Since no direct tracking was possible through periapsis using the HGA, high resolution gravity

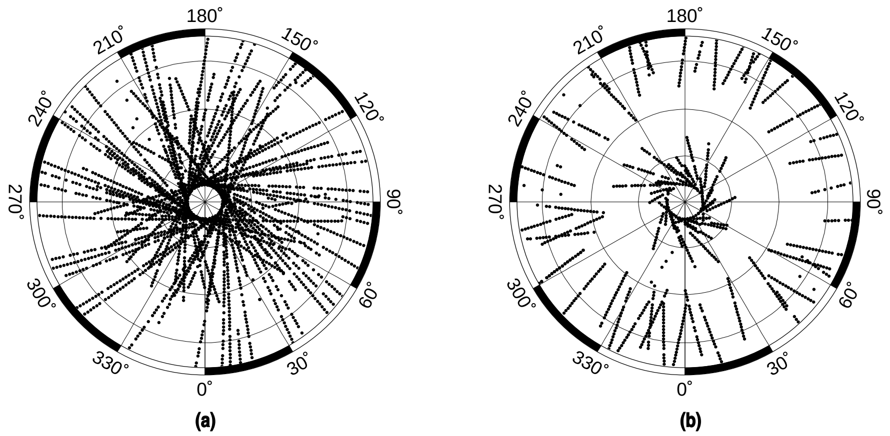

Figure 1: Geographic location of Doppler data acquired from Mars Global Surveyor, below 500 km altitude during SPO-1 and SPO-2 shown in a north pole stereographic projection to 55° N (a) Data acquired below 300 km. (b) Data acquired between 300 and 500 km altitude.

mapping of the Northern Hemisphere of Mars would have been compromised.

The orbits during SPO represented an unique opportunity, in that it would be possible for the first time to obtain high resolution gravity information over the northern polar regions of Mars from a relatively low altitude (170-300 km). Earlier low-altitude tracking data had been obtained in the 1970's from S Band tracking of the Viking Orbiters, but mostly from the equatorial regions of the planet[9,10,11].

The solution to the HGA Earth visibility problems during SPO-1 and early SPO-2 was to use the spacecraft low gain antenna (LGA). Special arrangements were made to collect one-way tracking data from the MGS Ultrastable Oscillator (USO)[5]. One-way Doppler differs from two and three-way Doppler in that the signal originates at the spacecraft. For two-way and three-way Doppler, the signal originates at an Earth tracking station, and is simply transponded by the MGS spacecraft[5,12]. One-way Doppler rather than two-way Doppler were obtained to prevent loss of valuable low-altitude data in the time it would take for the Earth tracking station to lock up on the signal from MGS in two-way mode. During SPO-1, valid one-way Doppler data were obtained starting three to eight minutes before periapsis. The spacecraft switched to the HGA again after the end of the periapse pass and the return to Array Normal Spin (ANS) attitude. During periapse passes in SPO-2, one-way data were obtained on nearly every other orbit through July 8, 1998. Two-way Doppler data over four periapse passes (389, 392, 396, and 398) in SPO-2 were obtained from the low gain antenna (LGA)[8]. The geographical distribution of the one-way Doppler data acquired during SPO-1 and SPO-2 is depicted in Figure 1.

Mars Global Surveyor was tracked primarily by the 34 m High Efficiency Antennae (stations 15, 45, 65), and the newer 34 m beam-waveguide (BWG) antennae (stations 34, 54, 25)[13] of the Deep Space Network (DSN). In addition to the one-way and two-way Doppler data, some passes of three-way Doppler data were obtained. Three-way Doppler differs from two-way Doppler in that different antennae are used for transmission and reception of the Doppler signal[12]. The averaging times for the two-way Doppler data was 60 seconds during Hiatus and SPO-1, and 10 seconds during SPO-2. For the one-way Doppler most of the data were averaged over 10 seconds.

FORCE AND MEASUREMENT MODELLING

Representation of the Gravitational Potential

The Mars gravity potential is modeled in spherical harmonics using the expression[14],

$$U = \frac{GM}{r} \sum_{l=0}^{\infty} \left(\frac{a_e}{r}\right)^l \sum_{m=0}^{l} \{\bar{C}_{lm} \cos m\lambda + \bar{S}_{lm} \sin m\lambda\} \bar{P}_{lm}(\sin\phi) \tag{1}$$

where the expansion is defined using the spherical coordinates of radius, r, latitude, ϕ, and longitude, λ; $\bar{C}_{lm}$ and $\bar{S}_{lm}$ represent the normalized geopotential coefficients; $\bar{P}_{lm}$ are the normalized associated Legendre functions of degree l and order m; a_e is the reference equatorial radius; G is the universal constant of gravitation, and M is the planet mass. A solution for the Mars gravity field consists of estimates for the coefficients $\bar{C}_{lm}$ and $\bar{S}_{lm}$ and the gravitational constant GM.

Definition of the Box-Wing Model

The nonconservative force model must take into account the complex geometry and material properties of the spacecraft. To that end, the spacecraft is treated as a combination of flat plates arranged in the shape of a box with attached solar arrays and drag flaps (ie. 'Box-Wing' or 'Macromodel'). The solar radiation pressure, atmospheric drag, and Mars albedo and infrared emission forces acting on each flat plate are computed and vectorially summed to compute the total nonconservative force acceleration acting on the spacecraft. The same approach has been used to model the nonconservative forces acting on other spacecraft, for instance TOPEX/Poseidon[15], and TDRSS[16]. Self shadowing of spacecraft elements is not considered. A fourteen plate box-wing model for MGS was derived for use during Hiatus and SPO from engineering drawings of the spacecraft.

The radiation pressure acting on a flat plate can be computed using the following equation, assuming Lambertian diffusion[17],

$$\Gamma_S = -\frac{GA\cos\theta}{Mc}[2(\delta/3 + \rho\cos\theta)\vec{n} + (1-\rho)\vec{s}]] \tag{2}$$

where Γ_S is the acceleration due to the solar radiation pressure on a flat plate, G is the radiation flux from the source (the Sun) in W/m^2, A is the surface area of the flat plate, M is the satellite mass, c is the speed of light, δ is the diffuse reflectivity (defined as a percentage of the incoming radiation), and ρ is the specular reflectivity (also defined as a percentage of the incoming radiation), θ is the angle between the surface normal and the solar incidence, $\vec{n}$ is the surface unit normal vector, and $\vec{s}$ is the unit vector from the source.

The albedo and infrared accelerations use a similar equation to equation(2), however the flux magnitude and source vector differ. The source is the vector from the Mars surface spot to the satellite. The spot definition and location are defined by Knocke et al.[18]. The Mars albedo and thermal emission is modelled using zonal spherical harmonic models of the Mars albedo and 3x3 spherical harmonic models of the planetary thermal emission as a function of Mars areocentric longitude, L_s[11]. In our implementation, we calculate the solar reflected radiation and planet thermal emission separately for 43 surface spots in three concentric rings and a central cap beneath the subsatellite point. The total albedo and infrared acceleration can be represented as,

$$\Gamma_A = -\sum_{i}^{N} \sum_{j}^{Jmax} \frac{G_j A_i \cos\theta_{ij}}{Mc}[2(\delta_i/3 + \rho_i \cos\theta_{ij})\vec{n} + i + (1-\rho_i)\vec{s}_j] \tag{3}$$

where the index i refers to plate i, and the summation takes place over N plates, the index j refers to the surface spot j, and the summation occurs over $Jmax$ surface spots. If the angle θ_{ij}, between the normals to the surface spot and the plate is greater than 90°, then the acceleration is not computed since the plate cannot observe the surface spot.

The atmospheric drag is computed according to the equation,

$$\vec{D} = -\frac{1}{2}\frac{C_D}{m}\rho\vec{v}|\vec{v}|\sum_{i}^{N} A_i \cos\theta \tag{4}$$

where C_D is the drag coefficient, ρ is the atmospheric density, and $\vec{v}$ is the satellite velocity with respect to the atmosphere. The angle θ is the angle between the plate normal unit vector and the spacecraft velocity vector.

MGS Attitude during Hiatus and SPO

The definition of a geometric model for the MGS spacecraft must be accompanied by specification of the spacecraft attitude, so that the forces perturbing spacecraft motion can be computed properly and so the tracking data can be corrected for the motion of the antennae with respect to the spacecraft center of mass. The GEODYN orbit determination (OD) software can calculate spacecraft orientation either using spacecraft quaternions or an internal attitude model[19]. However, the MGS spacecraft quaternions cannot be relied on exclusively since gaps occur in the quaternion data stream. Thus, it is important to understand the various spacecraft attitude regimes, and develop an analytical attitude model to 'fill-in' during the quaternion gaps.

The origin of the MGS spacecraft body-fixed coordinate system is located on the spacecraft-launch vehicle interface plane and the center axis of the spacecraft (ie. through the bottom center of the propulsion nozzle) (see Figure 2). The +Z axis is aligned with the nadir instrument deck, and +X axis points toward the stowed position of the HGA. The Y axis completes the orthogonal set.

During Hiatus and SPO, two attitude regimes predominated: nadir pointing and array normal spin (ANS). Near periapsis the spacecraft instrument panel (+Z face of the spacecraft) was usually pointed at nadir to collect science data. Far from periapsis the spacecraft was in array normal spin, with the high gain antenna (+X spacecraft body fixed axis) pointed at the Earth (see Figure 2), rotating once every 100 minutes about this axis. In addition, for up to sixty minutes per orbit, ANS was interrupted to turn the spacecraft and warm the MOLA instrument. On some periapse passes the instrument panel was deliberately pointed off nadir to acquire science data.

During the periapse passes in SPO-2, orbit geometry and low gain antenna viewing constraints dictated that the spacecraft be yawed such that the MGS spacecraft +Y axis was aligned with the velocity vector, so that the Earth could receive the one-way data from the low gain antenna. This yaw mode was implemented on every other revolution, with alternate revolutions devoted by the Mars Orbiter Camera (MOC) to targeted imaging. In addition during 12 passes, the nadir instrument panel was deliberately pointed as much as 49.2° off nadir so MOLA could acquire measurements over the center of the North polar cap*.

In our macromodel, we modelled the solar arrays as swept forward 30° in the +X direction, consistent with the mission documentation for the array normal spin attitude[20]. However, analysis of the spacecraft solar array quaternions shows that this cant angle varied between 23.95° and 33.68° between Insertion, Hiatus, and SPO. In addition, starting later in SPO-2, the attitude of the solar array was altered from nominal during periapsis passes.

It is evident that unlike mapping, the MGS spacecraft during SPO-1 and SPO-2 experienced a multitude of attitude regimes. An analytical or semi-empirical model that handled all contingencies and special circumstances (Phobos flybys for instance) would attain inordinate complexity. Therefore, as a first approximation, the analytical attitude algorithm modelled only the nadir attitude during the periapsis pass, and the ANS attitude far from periapsis, with the presumption that the

*If the MOLA instrument had remained nadir pointed, altimeter coverage in SPO would only have reached 86.3°N, because of the inclination of the MGS orbit.

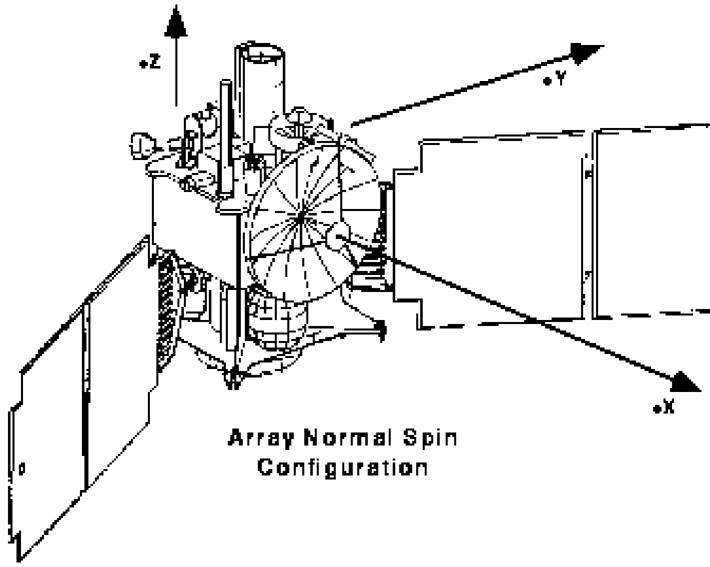

Figure 2: Nominal MGS spacecraft configuration during Array Normal Spin (Figure from ref. 20).

model would come into play only during quaternion data gaps, and that the spacecraft quaternions would handle off-nadir targeting passes, rollouts (transitions from nadir to ANS attitude), and MOLA warming maneuvers.

The fidelity of the macromodel is illustrated in Table 2, which summarizes the RMS of fit to the tracking data for 4.5 day arcs in SPO-1, using a box-wing model, and a 'cannonball.' In the absence of a macromodel, as far as the force model is concerned, the spacecraft is effectively modelled as a 'cannonball' with a constant cross-sectional area. The RMS of fit to the one-way Doppler data in these nine arcs improves by 0.64 mm/s or about 25 percent, with the macromodel.

It is not just the fit to the tracking data, but the actual orbit consistency which improves with the application of a macromodel. Successive 4.5 day arcs that overlapped by 12 hrs in SPO-1 (from 980327 to 980501) and SPO-2 (from 980531 to 980710) were used to compare modelling the MGS orbits with a cannonball and with a macromodel. No other aspect of the modelling, in terms of adjusted parameters or measurement model corrections, were changed in these tests. Once-per-revolution along-track empirical acceleration parameters were not adjusted in thes orbit tests. As summarized in Table 3, the application of the macromodel improves the orbit consistency by 15 percent (6 m) in the radial direction, and about 10 percent (70 m) in total position.

Measurement Offsets and Tracking Point Corrections

The MGS spacecraft has five antennae: a High Gain Antenna (HGA) and four low gain antennae (LGA's). Two of the LGA are reserved for transmission and two for reception. The HGA is not deployed until mapping, and is stowed next to the +X face of the spacecraft (see Figure 2). The coordinates of the geometric centers of these antennae are summarized in Table 4, and provided in a MOLA instrument kernel[21]. The coordinates refer to the MGS spacecraft body-fixed frame. The center of gravity of the spacecraft (or the offset of the center of mass from the origin of the spacecraft

Table 2: RMS of fit (in mm/s) for Arcs in SPO-1: Comparison of Macromodel vs. Cannonball [a]

Arc	No. of Doppler Obs.		Cannonball		Macromodel	
	1-way	2-way	1-way Dop.	2-way Dop.	1-way Dop.	2-way Dop.
980327	387	2524	2.66	0.46	1.71	0.46
980403	900	3098	1.64	0.44	1.11	0.44
980406	630	2243	1.64	0.54	1.31	0.54
980410	1420	3813	2.62	0.61	1.40	0.61
980413	875	1427	1.38	0.47	1.27	0.47
980417	1154	2929	2.91	1.06	1.54	1.07
980420	232	2605	1.41	1.72	1.40	1.72
980424	961	2941	3.31	1.81	2.04	1.82
980427	206	2283	1.76	2.15	1.76	2.14
Average			2.15	1.03	1.51	1.03

[a]The orbit determination results in this table were all computed with the MGM0890 (70x70) gravity model.

Table 3: Summary of Overlap Statistics in SPO-1 and SPO-2:
Cannonball vs. Macromodel

	Average RMS for 19 overlaps (meters)			
	Radial	Cross-track	Along-track	Total
Cannonball	39.1	542.8	454.2	773.1
Macromodel	33.2	505.8	399.9	701.8

body-fixed frame) must also be specified, and is also summarized in Table 4.

The two transmit LGA's are attached to the TWTA (traveling wave tube amplifier) box which is mounted on the HGA reflector. Hence, the coordinates for the transmit LGA's apply only while the HGA is stowed. The 'front' transmit LGA was used for transmission of one-way Doppler data during SPO-1 and SPO-2. The 'rear' transmit LGA was not used since its boresight is oriented about 160° from the +X axis[22].

To underscore the importance of applying the measurement model offsets for the one-way Doppler data, we show in Figure 3 the residuals for a short seven hour arc centered on periapsis 238 (April 14, 1998). In the first case the measurement offset corrections detailed in Table 4 were not applied, and the RMS reaches -6 mm/s. Although the spurious signal in the residuals occurs during a spacecraft roll-out (transition from nadir-pointing attitude to array normal spin) and at a relatively high altitude (approximately 2000 km), such a signal would corrupt the one-way Doppler data and their contribution to gravity field mapping. The RMS for this pass (consisting of 207 one-way Doppler observations) is 1.45 mm/s without the measurement model correction, and 0.84 mm/s when the

Table 4:MGS Antenna and CG Offset Corrections

	Coordinates (meters)		
	X	Y	Z
HGA (stowed)	0.999	0.000	1.680
LGA-transmit (front)	0.999	-0.716	2.069
LGA-transmit (back)	0.526	-0.763	2.072
LGA-receive (+X)	0.806	0.134	0.446
LGA-receive (-X)	-0.655	0.000	1.268
CG-Launch	-0.0010	-0.0007	1.1320
CG-Mapping	0.0298	0.0718	0.9970

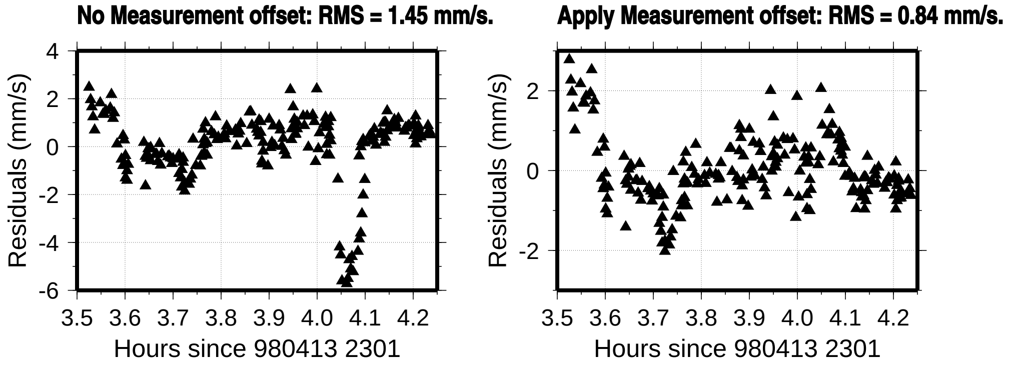

Figure 3: Effect of the measurement offset correction on one-way Doppler residuals for periapse pass 238 (April 14, 1998).

correction is applied. Not every periapsis pass has this dramatic a signature, but nevertheless the one-way Doppler data show substantial improvement when these corrections are applied. In contrast, the application of the measurement offset corrections change minimally the RMS of fit to the two-way Doppler data. This is logical since nearly all the two-way Doppler data were obtained on the HGA while the spacecraft was in array normal spin (hence Earth pointing). In this orientation, the measurement offset correction for the two-way Doppler data would not be discernible.

Other modelling issues

The MGS spacecraft must periodically fire its thrusters to desaturate the reaction wheels, which absorb angular momentum from disturbance torques acting on the spacecraft. These thruster firings can impart some velocity impulse (ΔV) to the spacecraft, effectively altering the spacecraft orbit. Nine angular momentum desaturation maneuvers were documented in Hiatus (October 13 to November 7, 1997), four in SPO-1 (March 27 to May 1, 1998), and sixteen in SPO-2 (May 31 - Sept. 23, 1998). In our orbit determination, a three-axis (radial, along-track, cross-track) constant acceleration is estimated over the duration of these maneuvers.

The DE403 planetary ephemerides were used as the source of ephemeris information for the measurement model, and for the calculation of the third body perturbations[23]. Solid tides raised by the Sun on Mars were also included using a k_2 Love number of 0.05 from Balmino et al.[9]. The Stewart atmosphere model was used to compute the atmospheric density[24]. The third body perturbations due to Phobos and Deimos were applied with an ephemeris from B. Jacobson[25] and GM values of 720,000 m^3/s^2 for Phobos[26], and 120,000 m^3/s^2 for Deimos[27†]. The orientation of Mars is computed using the 1991 system of IAU constants[28]. The DSN provides weather data in the form of temperature, barometric pressure, and relative humidity for each of the Deep Space Complexes at Goldstone, Madrid, and Canberra[29]. The weather data are provided to the MGS project at half-hour intervals. The weather data are interpolated to the appropriate transmit and receive times of each measurement, and an Earth troposphere refraction correction is applied to the tracking data using a Hopfield model[30].

The arcs in Hiatus, SPO-1, and SPO-2 were four to five days in length. The adjusted arc parameters included the spacecraft position and velocity; drag coefficients (once per orbit in Hiatus, and once every twelve hours in SPO); and a solar radiation reflectivity coefficient. Three axis

† MGS made several close (less than 1000 km) flybys of Phobos during SPO-1 and SPO-2, coming as close as 260 km on Sept. 12, 1998, when MOLA measurements were obtained from the satellite. The geometry of the MGS orbits during Hiatus and SPO did not favor 'close' approaches to Deimos, and the closest approach distance was 3000 km.

accelerations were estimated over the duration of any angular momentum desaturation maneuvers. Pass-by-pass biases were estimated for the range data. A frequency offset (f_b), as well as the first and second derivatives of this frequency offset with time($\dot{f}_b$ and $\ddot{f}_b$) were adjusted in each arc which included one-way Doppler data.

ORBIT DETERMINATION RESULTS

Gravity Model Determination

Data Used

The quality of the orbits computed for MGS during Hiatus and SPO is intimately associated with the Mars gravity model used to reduce the tracking data, and which satellites contributed to that gravity model's development. The first analysis of the SPO-1 and Hiatus data relied on GMM-1[10], a 50x50 model developed from a reanalysis of the Mariner 9 and Viking Orbiter tracking data. However, it was obvious that the determination of improved orbits for analysis of MOLA data, required that the MGS tracking data be incorporated into Mars gravity solutions. So, a sequence of models were developed that incorporated more MGS tracking data, and gradually refined the weights of both the new and the historical (Mariner 9 and Viking) tracking data. At several stages, the MGS tracking data used up until that point were reanalyzed with the newer MGS derived gravity model. New normal equations were created for the MGS data, and these 'updated' normal equations were included in the subsequent gravity model solutions. This process of iteration was essential, since the knowledge of the Mars gravity field in the northern polar regions was quite coarse prior to the start of the gravity mapping campaigns in SPO-1 and SPO-2. We report on the performance of five landmark models, to show the evolution in orbit performance: (1) GMM-1, the *a priori*, 50x50, solution from Mariner 9 and Viking Orbiter tracking[10]; (2) MGM0827E, a 70x70 solution incorporating only MGS data from SPO-1 in addition to the historical data; (3) MGM0883, a 70x70 solution that included the historical data, as well as most of the available MGS data in SPO-1 and SPO-2; (4) MGM0890, a 70x70 solution that added the remaining MGS data from SPO-2; (5) MGM0890a, a 80x80 solution identical in data content to MGM0890. The measurement offset correction was not applied in the orbit analysis prior to the derivation of the MGM0890 models. After the end of SPO-2, all the one-way Doppler passes were rescrutinized, and the data reedited after applying the measurement offsets discussed earlier. In addition, the one-way Doppler data were assigned an *a priori* sigma of 1.0 Hz (3.57 mm/s) in the orbit determination (OD) analysis for MGM0827E and MGM0883, but these data were upweighted and assigned an *a priori* sigma of 0.2 Hz (0.71 mm/s) in the orbit determination (OD) analysis for the MGM0890 series of solutions. The two-way and three-way Doppler data were assigned an *a priori* sigma of 0.1 Hz (0.36 mm/s) in all the OD analyses.

As a matter of interest, it is possible to derive a Mars gravity solution solely from the MGS tracking data in Hiatus and SPO, however the historical data are still needed to stabilize the solution at long wavelengths, and provide higher resolution information in regions not sampled at low altitude by MGS.

The MGM0827E and later models incorporated some changes in the historical (Mariner 9 and Viking Orbiter) data. All the newer models incorporated Mariner 9 data from April - July 1972, not included in GMM-1. In addition, Viking-1 Orbiter tracking from June and July 1976, as well as S Band range data to the Viking Orbiters were added in MGM0827E and subsequent solutions (see ref. 11 for a complete description of the historical data).

Table 5: Data Summary for Mars Gravity Solutions

Model	Number of Observations: Mariner 9	VO-1	VO-2	MGS	Comment
GMM-1 (50x50)	49,878	95,370	87,075	0	*Smith et al.* [1993].
MGM0827E (70x70)	69,992	109,844	74,373	61,270	Add MGS data to 98/05/01.
MGM0883 (70x70)	69,992	109,176	76,005	219,988	Add MGS data to 98/09/01.
MGM0890 (70x70)	69,992	109,176	79,545	257,165	Add MGS data to 98/09/17.
MGM0890a (80x80)	69,992	109,176	79,545	257,165	Same data used as MGM0890.

Method of Solution

The Mars gravity solutions were computed using least squares collocation[31,32] which minimizes the sum Q of signal and noise according to the relation,

$$Q = \sum_{l,m} \frac{\bar{C}_{lm}^2 + \bar{S}_{lm}^2}{\sigma_l^2} + \sum_t \sum_{obs_j} \frac{r_{ik}^2}{\sigma_k^2} f_k \tag{5}$$

where the signal is given by normalized spherical harmonic coefficients $\bar{C}_{lm}$ and $\bar{S}_{lm}$; $\sigma_l = 13.0 \text{ x } 10^{-5}/l^2$ is the RMS of the coefficients of degree l from the *a priori* power law based on the 18x18 solution of Balmino et al. (see ref. 9); r_{ik} is the observation residual for the i_{th} observation of satellite tracking data group k, and σ_k is the RMS of the observation residuals for data group k, and f_k is a downweighting factor to compensate for unmodelled error effects for each data group. Without some type of constraint in addition to the observation equations, the least squares solution would yield spherical harmonic coefficients with excessive power in the high degree terms. We apply a spectral constraint using a power law in the derivation of our gravity solutions, however other types of constraints are possible, for instance the spatial and spectral technique described by Konopliv and Sjogren in their derivation of the Mars50c gravity solution[33].

The method of Lerch[34] using subset solutions was applied to adjust the *a priori* weights of each data set. The essence of this method is that the aggregate changes in the spherical harmonic coefficients caused by the addition of an independent set of data should be commensurate with the aggregate change in the standard deviations of the spherical harmonic coefficients (See also ref. 35 for a detailed discussion of how the method was used to calibrate the relative weights of tracking data in a satellite-only solution for the Earth). The MGS data were grouped into four sets for purposes of calibrating the data: Hiatus, SPO-1, SPO-2 through June 30, 1998, and SPO-2 from July - Sept. 1998. The historical (Mariner 9 and Viking Orbiter) data were grouped according to satellite periapsis height and mission phase to determine their calibrations.

Orbit Performance

The orbit performance of these different gravity models can be evaluated by computing the orbit position discrepancy between overlapping arcs. The set of overlaps included nine 4.5 day arcs in SPO-1 form March 27-May 1,1998 and 23 4.5 day arcs in SPO2 from May 31-September 8, 1998. All arcs overlapped by only 12 hours, or just over one revolution of MGS about Mars. The orbits were compared every 20 seconds in the overlap interval. The overlap between the arcs starting on July 10 and July 14 was eliminated since the radial component was anomalously high (800-3000 m) for all the gravity models tested. The orbit overlaps are reported in Table 6. The radial orbit consistency was improved from 160 to 200 meters with the *a priori* GMM-1 to 30 - 36 meters with the most recent model including MGS data (MGM0890). For the SPO-2 orbits, the MGM0827E model (including MGS data from SPO-1) is already an improvement over the *a priori* GMM-1 model. Not surprisingly, though, the MGM0827E model has superior performance for the SPO-1 orbits (with an average RMS radial overlap of 39 m) than the SPO-2 orbits (with an average RMS radial overlap

Table 6: Orbit Overlap Statistics for Mars Gravity Models

Average RMS Overlaps for 9 Arcs in SPO-1 (m)				
Model	Radial	Cross-track	Along-track	Total
GMM-1	206.3	4951.9	2816.6	5741.8
MGM0827E	38.7	1819.6	1084.4	2132.2
MGM0883	36.5	1315.1	707.1	1503.1
MGM0890	35.9	934.1	424.0	1034.1
MGM0890a	35.1	923.5	418.2	1023.2
Average RMS Overlaps for 23 Arcs in SPO-2 (m)				
Model	Radial	Cross-track	Along-track	Total
GMM-1	164.1	1080.7	3641.3	3827.9
MGM0827E	98.1	839.9	2833.0	2980.6
MGM0883	32.3	220.3	775.5	814.4
MGM0890	29.1	116.5	491.2	510.5
MGM0890a	28.6	115.1	485.8	504.8

of 98 m). The improvement of the ensemble of SPO-1 and SPO-2 orbits required that all available MGS tracking be included in the gravity model solutions. The difference in orbit overlap quality between the MGM0890 (70x70) and MGM0890a (80x80) model is negligible. The RMS of fit to the tracking data also shows little change between the two models (see Table 7) implying that the extension of the field to 80x80 does not benefit the orbit determination for MGS.

The RMS of fit to the tracking data has been dramatically reduced (for example, from 39 mm/s with GMM-1 to 1.5 mm/s with MGM0890 for the one-way data) confirming that the signal in the tracking data has been substantially accommodated by the new gravity models. Nevertheless, the RMS of fit to the two-way and three-way Doppler data remains in excess of the nominal noise floor for the X Band Doppler data of 0.1 mm/s. In the vicinity of periapsis, systematic signals remain in the one-way Doppler residuals as well - some of them of high frequency as seen for example in Figure 4. We depict the two-way and three-way Doppler residuals from a 4.5 day arc starting on March 27, 1998 using GMM-1, and MGM0890. The one-way Doppler residuals are shown two periapse passes: 208, and 209. Whether, the high frequency signal depicted in the one-way Doppler residuals with MGM0890 is due to a surface gravity anomaly or whether it is due to other unmodelled effects remains to be established. Further improvements in the analysis of the Hiatus and SPO tracking data are still possible.

Evaluation of MGS Orbits Using Altimetry Crossovers

The orbits released to the MOLA science team were evaluated using altimeter crossovers‡. Strictly speaking this evaluation cannot be viewed solely as a test of the MGM0883 and MGM0890 gravity models, as other changes in the data processing have occurred in the creation of the two sets of MGS ephemerides during SPO. This evaluation is interesting, since it tests the orbit quality where MOLA data are available (near periapsis, below 785 km), whereas the orbit overlaps test the orbit consistency around the entire orbit.

Crossovers were computed internal to both SPO-1 and SPO-2, and an observation timing bias of 115.2 ms was applied. The roll and pitch offsets of the laser altimeter from the spacecraft body-fixed frame were set to values estimated in a SPO-1 tracking data and crossover orbit determination run (see the next section). The yaw offset of the MOLA altimeter from the spacecraft frame came from the MOLA instrument kernel[21]. The L1 (median absolute deviation normalized to unity for a gaussian) and L2 (root mean square deviation) norms were evaluated for the set of SPO-1 and

‡These orbits represent the gdn-ql06 series of orbits for MGM0883, and the gdn-ql09 series of orbits for MGM0890.

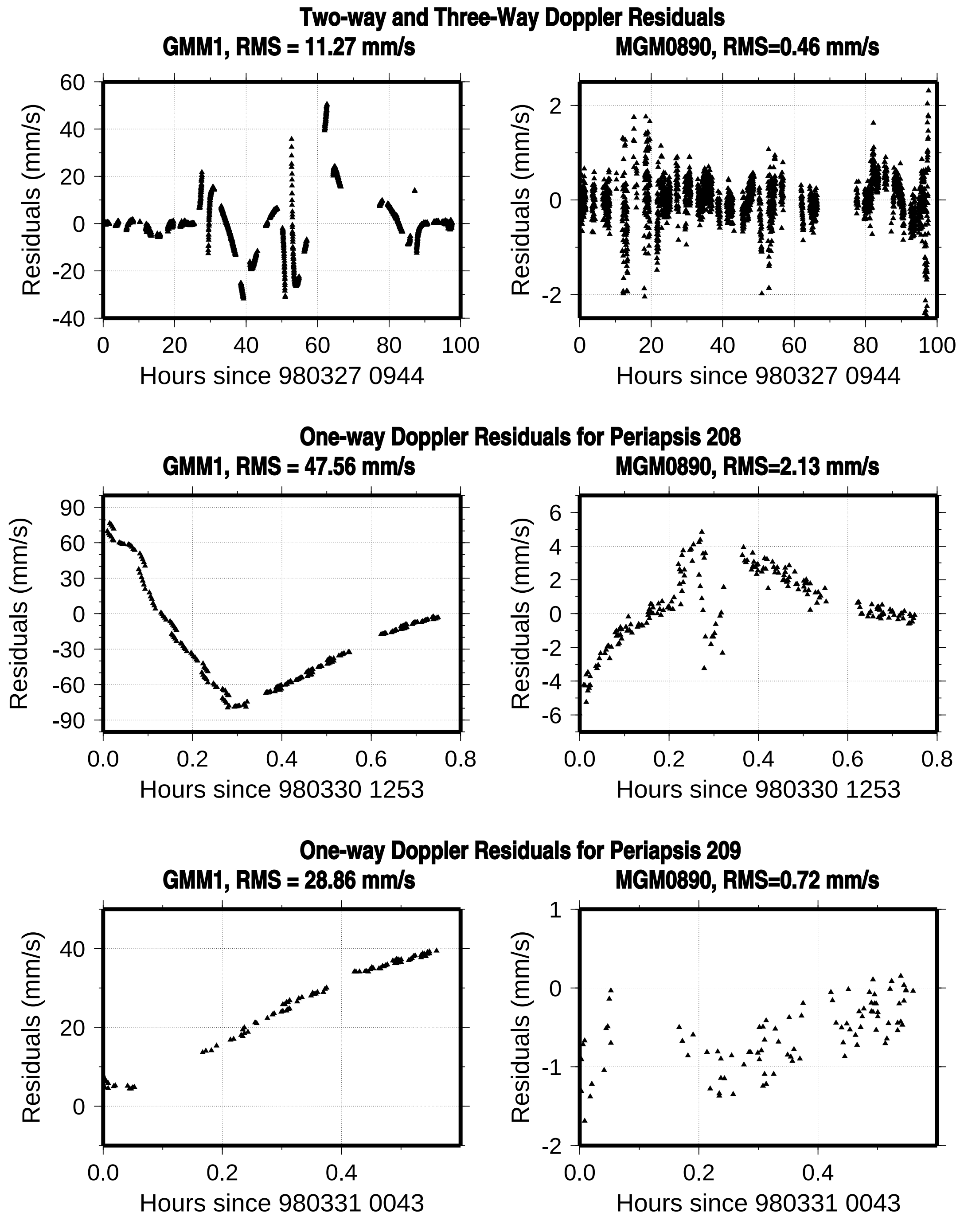

Figure 4: Doppler residuals for the 4.5 day arc starting on March 27, 1998 with the *a priori* GMM-1 (50x50) gravity model, and the MGM0890 (70x70), MGS-derived gravity model. The two and three-way Doppler residuals are shown for the entire arc. The one-way Doppler residuals from two periapsis passes in this arc are shown: periapsis 208 on March 30, 1998, and periapsis 209 on March 31, 1998.

Table 7: RMS of Fit for Mars Gravity Models

	RMS of Fit for 9 Arcs in SPO-1		
Model	1-way Doppler (mm/s)	2-way Doppler (mm/s)	2-way Range (m)
GMM-1	39.94	9.12	111.2
MGM0827E	4.88	1.28	29.7
MGM0883	2.64	1.06	29.0
MGM0890	1.51	1.03	29.0
MGM0890a	1.52	1.03	29.0
	RMS of Fit for 27 Arcs in SPO-2		
Model	1-way Doppler[a] (mm/s)	2-way Doppler (mm/s)	2-way Range (m)
GMM-1	14.06	5.15	67.9
MGM0827E	5.42	2.82	36.7
MGM0883	2.27	0.77	28.3
MGM0890	2.16	0.63	28.0
MGM0890a	2.31	0.62	28.0

[a]Only nine arcs in SPO-2 had 1-way Doppler data, so for this data type, the average is only computed over those arcs.

Table 8: Orbit Evaluation Using Altimeter Crossovers

	SPO-1	
	MGM0883	MGM0890
L2	63.9	61.6
L1	10.1	9.5
N[a]	1188	1189
	SPO-2	
	MGM0883	MGM0890
L2	141.9	70.9
L1	38.3	13.9
N	5879	5875

[a]N = number of crossovers.

SPO-2 crossovers, and are summarized in Table 8.

The orbits show slight improvement in SPO-1 (about 0.6 m or five percent as measured by the L1 norm), but a substantial improvement in SPO-2 (about 26 m or 67 percent, as measured by the L1 norm). The L2 norm is so much larger than L1 because of the presence of large tails in the crossover distribution.

Use of Altimetry Crossovers In OD for SPO-1

We experimented with using the MOLA altimetry directly to improve orbit determination for MGS. The motivation arises from the fact that an altimeter crossover observation provides a powerful constraint that ties together two separate orbit tracks. Altimetry in the form of crossovers has often been used to provide a constraint to orbit solutions (for example to Earth orbiting satellites such as GEOSAT, ERS-1 and ERS-2). When altimetry observations are used to form crossover constraint equations, less knowledge about the planet surface is required than when the alimeter data are used directly to form observation equations. See ref. 36 for a detailed discussion of the use of altimeter crossover constraint equations in orbit determination.

Conditions during Hiatus and SPO were quite different from those under which crossover constraints have usually been applied. Previously, crossovers have usually been used (1) over relatively flat surfaces such as oceans and ice sheets, (2) with radar altimeters that have a large footprint, (3) with satellites in a circular orbit, and (4) with satellites whose trajectories have already been well determined from conventional tracking (excluding altimetry).

Under conditions (1-3) above, crossover constraints are relatively insensitive to the horizontal (non-radial) components of orbit error. Because of this relative insensitivity to horizontal orbit error and also because the satellite trajectories have already been well determined, crossover constraints have always been formulated in terms of surface height discrepancies at predetermined latitudes and longitudes. For MGS, the altimeter data is obtained in part at least over sloping topography, the laser altimeter has a narrow footprint (on the order of 100 m rather than many km), and the orbit is highly eccentric. In addition, the MGS orbit still has large orbit error even with the improvements described in the previous sections. Because of these differences, we are sensitive to horizontal (non-radial) orbit error, and therefore, we have formulated our crossover constraint equations differently. The crossover constraint formulation is described in ref. 37 so we will only summarize the main differences with the standard approach:

We define the crossover discrepancy to be the minimum distance between two curves of geolocated altimeter bounce points that have been traced out on the planet surface. The two curves correspond to the ascending and descending passes that surround a conventional crossover. The planet fixed coordinates of points on the curves are determined (geolocated) using orbit and attitude information, as well as the altimeter ranges. Our technique to minimize the crossover discrepancies does not assume that a crossover will occur in exactly the same location after the orbit parameters adjust in an OD solution. In fact, the constraint equations are written in a way that allow topography along the curves to be considered. The use of topography can influence the adjustment of orbit and attitude parameters so that the geolocated curves are relocated. Conversely, since the attitude influences the geolocation of altimeter bounce points, we can solve for attitude parameters using the the altimeter crossovers.

The short passes of altimeter data (20-30 minutes for a revolution of 11 hours and 38 minutes) available during SPO cause a complication in the use of the crossovers. The number of crossovers internal to a single arc (four or six days in length) is limited and it becomes impractical to rely solely on these 'intra-arc' crossovers. Therefore, we combined six-day arcs spanning all of SPO-1 into a single simultaneous multi-arc solution using ground tracking and altimeter crossovers. Bringing in 'inter-arc' crossovers in this fashion makes it possible to use hundreds of crossovers.

Two types of solutions were obtained using the altimeter crossovers in SPO-1. In the first solution, 279 off-nadir crossovers (where either the ascending or descending pass pointed more than 2° off-nadir) were used to solve for attitude parameters, while the orbit was held fixed to the orbit solution determined solely from the tracking data. The 535 most nadir pointing crossovers were used simultaneously with the ground tracking observations in an orbit solution. In this second solution, the attitude parameters were held fixed to the the values obtained from the first (attitude parameter) solution.

Three parameters were estimated in the 'attitude only' crossover solution. The first is a time tag bias for the telemetered quaternions that describe the spacecraft orientation. The other two are constant roll and pitch offset parameters that describe the orientation of the MOLA instrument in the spacecraft body frame. The sense of these parameters is that a a vector in the spacecraft body fixed frame is rotated to the MOLA instrument frame by successively applying rotations in roll, pitch, and yaw. The preflight values of the parameters were 0.021° for roll, -0.005° for pitch and 0.059° for yaw[21]. In flight, these parameters can also help compensate for offsets in the the telemetered quaternions that describe the spacecraft body orientation. Using the 279 SPO-1 off-nadir crossovers in the 'attitude-only' solution, we find a timing bias in the MGS spacecraft telemetered quaternions of 1.160 seconds, a roll offset of -0.0028°, and a pitch offset of -0.0086°. In ref. 37 it is demonstrated

Table 9: RMS Orbit Overlaps Using Altimeter Crossovers

	RMS Orbit Overlaps (m)			
Solution type	Radial	Cross-track	Along-track	Total
No crossovers	18.5	907	505	1045
Include crossovers	15.8	347	201	402

that the use of these adjusted attitude parameters improve the pointing of the MOLA instrument, at least during SPO-1.

To evaluate the effect of the 535 nearly nadir altimeter crossovers on the determination of the MGS orbit, we compute the RMS orbit discrepancies for each of the six-day arcs (which all overlap by 12 hours) after obtaining the multi-arc solution. These nadir crossover orbit solutions also included an estimate for a MOLA altimeter timing bias and we obtained a value of 113.6 ± 1.0 msecs. The crossover solution is compared to a solution that relied solely on the DSN tracking data (Doppler and range). (see Table 9). Note that the radial orbit overlaps for the 'tracking-data-only' solutions are superior (18 m compared to 30 m) then those cited in the gravity model tests (compare with Table 6) since empirical once-per revolution parameters were adjusted frequently in the crossover arcs.

The crossovers improve the radial orbit consistency in SPO-1 by 15 percent (2.8 m), and 60 percent (600 m) in total position. Although the radial component is only slightly improved, the along-track and cross-track components of the orbit are improved substantially. This multiarc crossover solution strategy can also be applied in SPO-2 and Hiatus, although the Hiatus period has no internal crossovers. Hiatus arcs must be adjusted together with SPO arcs in order to allow the crossovers to improve the Hiatus orbits. Once mapping commences from the low-altitude, near-circular, and polar orbit, sufficient altimeter data should be available to rely solely on 'intra-arc' crossovers.

SUMMARY

The Doppler tracking data from Mars Global Surveyor in Hiatus and the Science Phasing Orbits have been incorporated into updated models of the gravity field of Mars. These solutions, to 70x70 in spherical harmonics, have been used to compute refined orbits for analysis of the MOLA altimeter data. The RMS radial orbit differences of overlapping arcs have been reduced from 160 to 200 m with the *a priori* GMM-1 model to 30 to 35 meters with the latest MGS derived solution, MGM0890.

For the first time we have used laser altimetry about another planet in the form of crossovers as a tool to strengthen determination of a spacecraft orbit. The use of crossovers during SPO-1 slightly improved the orbits in the radial direction, but improved them most especially in the along-track and cross-track directions.

Further improvements in the orbits of MGS during Hiatus and SPO will result from improving the macromodel to account for the articulation of the solar arrays, and the incorporation of the altimeter crossovers into the Mars geopotential solutions.

ACKNOWLEDGEMENTS

We acknowledge Theodore Moyer of JPL for providing information regarding the modelling of the interplanetary one-way Doppler data; Phil Tracadas of MIT and Michael Griffin of Lockheed Martin provided information to help define the MGS macromodel. Susan Fricke of Raytheon ITSS provided computational support with GEODYN, and John McCarthy of Raytheon ITSS supported the gravity field development with SOLVE. We thank the NASA Center for the Computational Sciences (NCCS) at GSFC for hosting our gravity model solution development on their Cray J90 supercomputers. This work was supported by the Mars Global Surveyor Project.

REFERENCES

1. Albee, A. L., Mars Global Surveyor Mission: Status and Plan for Attaining the Circular Mapping Orbit, *EOS Trans. Am. Geophys. Un., 79*, 1998.

2. Esposito, P. B., V. Alwar, S. Demcak, E. Graat, M. Johnston, and R. Mase, Mars Global Surveyor: Navigation and Aerobraking at Mars, *AAS Paper 98-384*, 1998.

3. Zuber, M. T., et al., The Mars Observer Laser Altimeter Investigation, *J. Geophys. Res., 97*, 7781-7797, 1992.

4. Afzal, R. S., Mars Observer Laser Altimeter: Laser Transmitter, *Applied Optics, 33*, 3184-3188, 1994.

5. Tyler, G. L., et al., Radio Science investigations with Mars Observer, *J. Geophys. Res., 97*, 7759-7779, 1992.

6. Moyer, T. D., Changes to the ODP and ODE for processing X-Band uplink data, *Jet Propulsion Lab. Eng. Mem., 314-430,* 1987.

7. Moyer, T. D., REGRES Modifications for processing Block V exciter range observables, *Jet Propulsion Lab. Eng. Mem., 314, 5-1795,* 1995.

8. Priest, P., MGS Radio Science Support Team, Jet Propulsion Laboratory, Pasadena, California, Personal communications, April 1998 - January 1999.

9. Balmino, G., B. Moynot, and N. Valès, Gravity field model of Mars in spherical harmonics up to degree and order eighteen, *J. Geophys. Res. 87(B12)*, 9735-9746, 1982.

10. Smith, D. E., F. J. Lerch, R. S. Nerem, M. T. Zuber, G. B. Patel, S. K. Fricke, and F. G. Lemoine, An improved gravity model for Mars: Goddard Mars Model 1, *J. Geophys. Res., 98(E11)*, 20871-20889, 1993.

11. Lemoine, F. G., *The Dynamics of Orbiting Satellites and Gravity Model Development*, Ph.D. Thesis, The University of Colorado at Boulder, Boulder, Colorado, 1992.

12. Moyer, T. D., Mathematical formulation of the double precision orbit determination program (DPODP), *JPL Technical Report 32-1527*, Jet Propulsion Laboratory, Pasadena, California, 1971.

13. Deep Space network/Flight Project Interface Design Handbook, ed. by R. W. Sniffin, JPL Document 810-5, Rev.D; Vol.1, TCI-31, July 1, 1998.

14. Kaula, W. M., *Theory of Satellite Geodesy*, Blaisdell, Waltham, Mass., 1966.

15. Marshall, J. A. M., and S. B. Luthcke, Radiative Force Model Performance for TOPEX-Poseidon Precision Orbit Determination, *J. Astronautical Sciences 42(2)*, 229-246, 1994.

16. Luthcke, S. B., J. A. Marshall, S. C. Rowton, K. E. Rachlin, C. M. Cox, and R. G. Williamson, Enhanced radiative force modelling of the Tracking and Data Relay Satellites, *J. Astronautical Sciences 45(3)*, 349-370, 1997.

17. Milani, A., A. M. Nobili, and P. Farinella, *Non-Gravitational Perturbations and Satellite Geodesy*, Adam Hilger, Briston, U. K., 1987.

18. Knocke, P. C., Ries, J. C., and B. D. Tapley, Earth radiation pressure effects on satellites, *Proceedings of the AIAA/AAS Astrodynamics Conference*, Minneapolis, Minnesota, AIAA Paper 88-4292, 577-588, August 1988.

19. Pavlis, D. E., S. Luo, P. Dahiroc, J. J. McCarthy, and S. B. Luthcke, GEODYN operations manuals, five volumes, Raytheon ITSS contractor report, December 18, 1998.

20. Mars Global Surveyor Project: Mission Plan, Final Version, Rev. B (MGS 542-405), edited by Wayne Lee, Jet Propulsion Laboratory, Pasadena, California, November 1996.

21. Semenov, B., Mars Orbiter Laser Altimeter Instrument Kernel, version 2.3, Navigation Ancillary Information Facility (NAIF), Jet Propulsion Laboratory, Pasadena, California, January 16. 1999.

22. Whetsel. C. W., Personal communication, Jet Propulsion Laboratory, October 27, 1998.

23. Standish, E. M., X X Newhall, J. G. Williams, and W. M. Folkner, JPL Planetary and Lunar Ephemerides, DE403/LE403, JPL Interoffice Memorandum 314.10-127, Jet Propulsion Laboratory, Pasadena, California, May 22, 1995.

24. Stewart, A. I. F., Revised time dependent model of the Martian atmosphere for use in lifetime and sustenance studies, Final report, JPL PO NQ-802429, Laboratory for Atmospheric and Space Physics, The University of Colorado, March 26, 1987.

25. Jacobson, R. A., Mar033-5 Phobos and Deimos ephemerides description, Jet Propulsion Laboratory, Sept. 29, 1997.

26. Kolyuka, Y. et al. International project Phobos, experiment: Celestial mechanics, *Planet. Space Sci., 39*, 349-354, 1991.

27. Williams, B. G., et al.,Improved determination of the Phobos and Deimos masses from Viking, Fall meeting of the American Geophysical Union, G21-A-11, San Francisco, December 1981.

28. Davies, M. E., et al., Report of the IAU/IAG/COSPAR working group on cartographic coordinates and rotational elements of the planets and satellites: 1991, *Celestial Mechanics and Dyn. Astr. 53*, 377-397, 1992.

29. DSN Flight Project Interface Design Handbook 810-5, Module MED-10, Media calibration, P. Richter ed., Nov. 15, 1992.

30. Tropospheric effect on electromagnetically measured range: prediction from surface weather data, *Radio Science 6(3)*, 357-367, 1971.

31. Schwartz, K. P., Least squares collocation for large systems, *Bull. Geod. Sci. 35*, 309-324, 1976.

32. Schwartz, K. P., "On the application of least-squares collocation models to physical geodesy," in *Approximation Methods in Geodesy*, edited by H. Moritz and H. Sunkel, 89-116, H. Wichmann-Verlag, Karlsruhe, Germany, 1978.

33. Konopliv, A. S., and W. L. Sjogren, The JPL mars gravity field, Mars50c, based upon Viking and Mariner 9 Doppler tracking data, *JPL Publication 95-5*, Jet Propulsion Laboratory, Pasadena, California, February 1995.

34. Lerch, F. J., Optimum data weighting and error calibration for estimation of gravitational parameters, *Bull. Geod. 65*, 44-52, 1991.

35. Lemoine, F. G., et al., *The Development of the Joint NASA GSFC and the NIMA Geopotential Model EGM96*, NASA/TP-1998-206861, NASA Goddard Space Flight Center, Greenbelt, Maryland, July 1998.

36. Shum, C. K., K. Zhang, B. Shutz, and B. D. Tapley, Altimeter crossover methods for precision orbit determination and the mapping of geophysical parameters, *J. Astronautical Sciences, 38(3)*, 355-368, 1990.

37. Rowlands, D., D. E. Pavlis, F. G. Lemoine, G. A. Neumann, and S. B. Luthcke, The use of laser altimetry in the orbit and attitude determination of Mars Global Surveyor, *Geophys. Res. Lett.*, manuscript in review, 1999.